J Solid State Electrochem (2012) 16:2739–2749
DOI 10.1007/s10008-012-1693-8

ORIGINAL PAPER

Mesoporous MnO_2 synthesized by hydrothermal route for electrochemical supercapacitor studies

Prasant Kumar Nayak · N. Munichandraiah

Received: 28 December 2011 / Revised: 3 February 2012 / Accepted: 13 February 2012 / Published online: 3 March 2012

Abstract Poorly crystalline mesoporous MnO_2, which is suitable for supercapacitor studies, is synthesized from neutral $KMnO_4$ aqueous solution by hydrothermal route. But it requires a high temperature (180 °C) and also a long reaction time (24 h). Addition of a tri-block copolymer, namely, poly(ethylene glycol)-block-poly(propylene glycol)-block-poly(ethylene glycol) (P123), which is generally used as a soft template for the synthesis of nano-structured porous materials, reduces the hydrothermal temperature to 140 °C and also reaction time to 2 h. When the reaction time is increased, the product morphology changes from nanoparticles to nanorods with a concomitant decrease in BET surface area. Also, the product tends to attain crystallinity. The electrochemical capacitance properties of MnO_2 synthesized under varied hydrothermal conditions are studied in 0.1 M Na_2SO_4 electrolyte. A specific capacitance of 193 Fg^{-1} is obtained for the mesoporous MnO_2 sample consisting of nanoparticle and nanorod mixed morphology synthesized in 6 h using P123 at 140 °C.

Keywords Mesoporous · Manganese dioxide · Nanoparticles · Nanorods · Surface area · Specific capacitance

Introduction

Electrochemical capacitors (ECs) or supercapacitors have attracted great attention in recent years owing to their higher power density and longer cycle life than batteries and higher energy density than conventional capacitors [1]. Although hydrous RuO_2 exhibits a high specific capacitance (788 Fg^{-1}), high cost and toxicity of RuO_2 limit its application [2]. MnO_2 is an alternative, promising electrode material for ECs as it is electrochemically active, inexpensive, abundant in nature, and environmentally friendly [3–33]. MnO_2 exists in different crystallographic forms, namely, α, β, γ, δ and λ, depending on how the MnO_6 octahedra units are interlinked with each other. Among these crystallographic structures, α- and δ-forms of MnO_2 are suitable for capacitor studies because of the presence of a sufficient gap in their structures for doping/undoping of cations from the electrolyte [3]. The electrochemical properties of MnO_2 also depend on the textural properties including morphology [4], porosity [5], and loading level of MnO_2 on current collectors. Transition metal oxides studied as alternates to RuO_2 also include NiO [34, 35], Co_3O_4 [36], Fe_3O_4 [37], and V_2O_5 [38] in addition to MnO_2.

Different routes for the synthesis of nano-structured MnO_2 include co-precipitation [6–8], sol–gel [9, 10], microemulsion [11], hydrothermal [12–17], and electrochemical methods [18–21]. Hydrothermal route is considered as a low temperature synthetic technique for the preparation of inorganic compounds. In this route, the reaction is carried out with the reactants present in an aqueous solution at a temperature usually between 100 and 200 °C under autogenerated pressure in a sealed container. The hydrothermal synthesis method is useful to tune the particle size, porosity, and morphology of reaction products by controlling reaction conditions. Preparation of crystalline MnO_2 was first reported by Chen et al. [17] from an acidic $KMnO_4$ solution at 170 °C for 4 days by hydrothermal route. Plate-like and nanorods of MnO_2 were synthesized hydrothermally by reaction between $KMnO_4$ and $MnSO_4$ by varying the

P. K. Nayak · N. Munichandraiah (✉)
Department of Inorganic and Physical Chemistry,
Indian Institute of Science,
Bangalore 560012, India
e-mail: muni@ipc.iisc.ernet.in

reaction time [13]. Recently, δ-MnO_2 with flower-like morphology was synthesized by a microwave-assisted hydrothermal method from an acidic solution consisting of $KMnO_4$ [22].

For supercapacitor studies, poorly crystalline MnO_2 is preferable than crystalline form [11]. In the present study, poorly crystalline mesoporous MnO_2 was synthesized hydrothermally from an aqueous solution of $KMnO_4$ without using any reducing agent or acidic condition. It required 180 °C and 24 h of hydrothermal reaction time. It was observed that MnO_2 did not form at lower temperatures and shorter reaction times. However, when poly(ethylene glycol)-block-poly(propylene glycol)-block-poly(ethylene glycol) tri-block copolymer (P123) was added to $KMnO_4$ solution, the formation of MnO_2 was observed at a lower temperature (140 °C) and in a shorter reaction time (2 h) under hydrothermal conditions. P123 is generally employed as a soft template for synthesis of nano-structured and porous materials [23]. However, morphology, surface area, and pore size were found to vary by increasing the reaction time at 140 °C. Supercapacitor properties of several MnO_2 samples prepared by varying hydrothermal reaction time were studied in 0.1 M Na_2SO_4 electrolyte.

Experiment

Analytical grade chemicals, namely, anhydrous $KMnO_4$ (SD Fine Chem.), anhydrous Na_2SO_4 (Merck), and Pluronic P123 (Aldrich), were used as received. Doubly distilled (DD) water was used for preparation of all solutions.

Synthesis of MnO_2

In a hydrothermal method, an aqueous solution of $KMnO_4$ (0.5 g $KMnO_4$ in 60 ml DD water) was transferred into a Teflon-lined stainless steel autoclave (volume 120 ml), held at 180 °C for 24 h, and then allowed to cool down to room temperature. Several attempts were made to synthesize MnO_2 at lower temperatures than 180 °C as well as shorter reaction times than 24 h. It was found that the product did not form, and 180 °C and 24 h were the minimum hydrothermal reaction conditions needed for the formation of MnO_2 from $KMnO_4$ in the absence of a reducing agent. In order to reduce the reaction time as well as the temperature, P123 was added to $KMnO_4$. For this purpose, 5.5 g of P123 was dissolved in 60 ml DD water with continuous stirring. To this, 0.5 g $KMnO_4$ was added and the reactants were stirred. The solution was then transferred into a Teflon-lined stainless steel autoclave (volume 120 ml), held at 140 °C for 2 h, and then allowed to cool down to room temperature. The product was filtered, washed several times in DD water at 60 °C, finally with ethanol to remove the excess P123, and then dried at 60 °C for about 6 h. By using P123, several samples of MnO_2 were prepared by increasing the hydrothermal reaction time to 6, 12, and 24 h.

Characterization and electrochemical measurements of MnO_2

The crystal structure was characterized by powder X-ray diffraction on a Bruker D8 Advance X-ray diffractometer using Cu K_α (λ=1.5418 Å) as the source. The morphology of the samples was investigated by a FEI Co. scanning electron microscope (SEM) model Sirion and transmission electron microscope (TEM) model T20. The samples for TEM studies were prepared by sonicating the sample in acetone, placing a few drops on a Cu grid, and drying under vacuum. The chemical composition and oxidation state of Mn on the surface of the nanostructure was examined by Thermo Fisher Scientific X-ray photoelectron spectroscopy (XPS) using X-ray Al anode (monochromatic K_α X-rays at 1,486.6 eV) as the source. The C 1S region was used as the reference and was set at 284.6 eV. For XPS studies, pallets were made from the powder samples and heated at 100 °C under vacuum for 6 h. Nitrogen adsorption/desorption experiments were carried out at 77 K by means of a Micromeritics surface area analyzer model ASAP 2020. The surface area values were calculated by using the Brunauer–Emmett–Teller (BET) method using multiple points of adsorption isotherm and pore-size distributions were calculated by the Barrett–Joyner–Halenda (BJH) method. The BET surface area values were calculated in p/p^0 range of 0.05–0.25 from adsorption branches of the isotherms. The BJH pore-size distributions were calculated from desorption branches of the isotherms. Samples were heated at 100 °C for 2 h under vacuum prior to surface property measurements.

For electrochemical studies, electrodes were fabricated on a high purity grade 304 stainless steel (SS) foil of 0.2 mm thickness as the current collector. Before fabrication, SS foil was polished with successive grades of emery and washed thoroughly with detergent, etched in dil. HCl, washed with running water, rinsed with DD water and then with acetone, and dried in air. MnO_2 (70 wt.%), Ketjen black EC-600 JD (Akzo Noble Polymer Chemicals) (20 wt.%), and poly (vinylidene fluoride) (Aldrich) (10 wt.%) were mixed, ground in a mortar, and a few drops of *n*-methyl pyrrolidinone was added to get a syrup. The syrup was coated on the pretreated SS foil of 1.0 cm^2 area and dried at 100 °C under vacuum for 12 h to achieve a loading level of 0.5–0.6 mg cm^{-2}. A Mettler Toledo electronic balance model AB265-S/FACT with 0.01 mg sensitivity was used for weighing the electrodes. The electrochemical studies were performed in a glass cell of about 50 ml volume, which had provision to introduce MnO_2-coated SS as the working electrode, Pt foils as the counter electrodes, and saturated calomel electrode (SCE) as

the reference electrode. An aqueous solution of 0.1 M Na_2SO_4 was used as the electrolyte. An Eco-Chemie potentiostat/galvanostat model Autolab PGSTAT 30 was used for all the electrochemical studies. All potential values were reported with respect to SCE. All experiments were conducted in an air-conditioned room at 22±1 °C.

Results and discussion

The hydrothermal synthesis technique involves subjecting the reactants to a temperature usually between 100 and 200 °C under auto-generated pressure in a sealed container. Due to the variation in the properties of water with change in temperature and pressure, the reaction conditions are critical in deciding the properties of the products [17, 24]. Subramanian et al. had synthesized MnO_2 hydrothermally by reaction between $KMnO_4$ and $MnSO_4$ [12]. Chen et al. had prepared $K_{0.25}MnO_2{\cdot}0.6\ H_2O$ by hydrothermal reaction of $KMnO_4$ in acidified H_2O at 170 °C for 4 days [17]. Layered MnO_2 with flower-like morphology was synthesized in an acidic condition (pH=2) by a microwave-assisted hydrothermal method [22]. However, in the present study, MnO_2 is synthesized hydrothermally from a neutral aqueous solution of $KMnO_4$ without the use of reducing agent or acidic conditions. The formation of MnO_2 required a temperature of 180 °C and duration of 24 h. In the absence of any conventional reducing agent, H_2O itself acts as a reducing agent at high pressure generated in the autoclave. The reaction involving the formation of MnO_2 is written as:

$$2\ KMnO_4 + H_2O \rightarrow 2\ MnO_2 + 2\ KOH + (3/2)O_2 \uparrow \quad (1)$$

A similar reaction was proposed by Chen et al. for preparation of $K_{0.25}MnO_2{\cdot}0.6\ H_2O$ by hydrothermal reaction of $KMnO_4$ in acidified H_2O at 170 °C for 4 days [17]. The MnO_2 sample synthesized in the hydrothermal method at 180 °C for 24 h without using any reducing agent is referred to as S180-24. In order to synthesize MnO_2 hydrothermally in a shorter duration and at lower temperature, P123 was used as the reducing agent. Generally, Pluronic P123 is used as a structure-directing agent for synthesizing porous materials [23, 25]. Pluronic P123 ($EO_{20}PO_{70}EO_{20}$) is an amphiphilic tri-block copolymer containing both hydrophilic poly(ethylene oxide) (PEO) and hydrophobic poly (propylene oxide) (PPO) groups. Due to the presence of both hydrophilic and hydrophobic groups in the polymer, it can form micelles in aqueous solutions and helps in the formation of nano-structured materials such as nanoparticles, nanorods, nanowires, nanofibers, etc. As MnO_2 was synthesized from the reduction of $KMnO_4$ by reducing agents such as fumaric acid [10], KBH_4 [26], alcohols, and glycols [27, 28], it was found that P123 containing terminal alcoholic groups also reduces $KMnO_4$ to MnO_2 [29]. By using P123, MnO_2 was synthesized at a lower temperature of 140 °C in 2 h only. For studying the effect of reaction time, several batches of 60 ml solution consisting of 0.5 g $KMnO_4$ and 5.5 g P123 were subjected to hydrothermal conditions at 140 °C for 2, 6, 12, or 24 h. MnO_2 samples synthesized by this method are respectively referred to as S140-2, S140-6, S140-12, and S140-24. In the synthesis of MnO_2 from $KMnO_4$ and P123, the polymer itself acts as a mild reducing agent. But the hydrothermal conditions made the reaction faster and on extended reaction times, the structure-directing nature of P123 was clearly noticed, as detailed below. Unlike acidic conditions [17] and reaction between $KMnO_4$ and $MnSO_4$ [12] reported previously for the synthesis of MnO_2 by hydrothermal route, neutral conditions in the absence as well as in the presence of P123 are employed in the present study.

XRD studies

The phase of the as-synthesized samples was examined by recording powder XRD patterns, which are shown in Fig. 1. There are only three broad peaks observed for the samples (except for S140-24) at 2θ=13°, 37°, and 66° which are

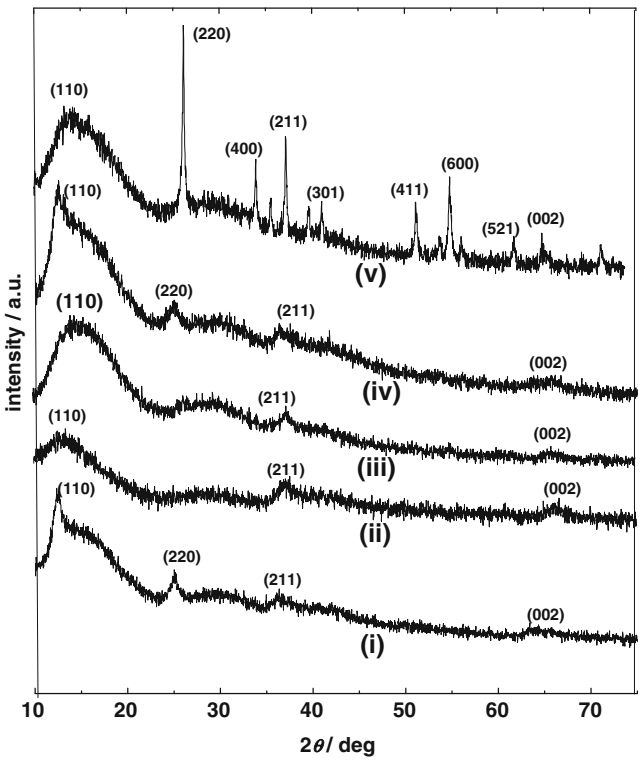

Fig. 1 XRD patterns of MnO_2 samples *(i)* S180-24, *(ii)* S140-2, *(iii)* S140-6, *(iv)* S140-12, and *(v)* S140-24

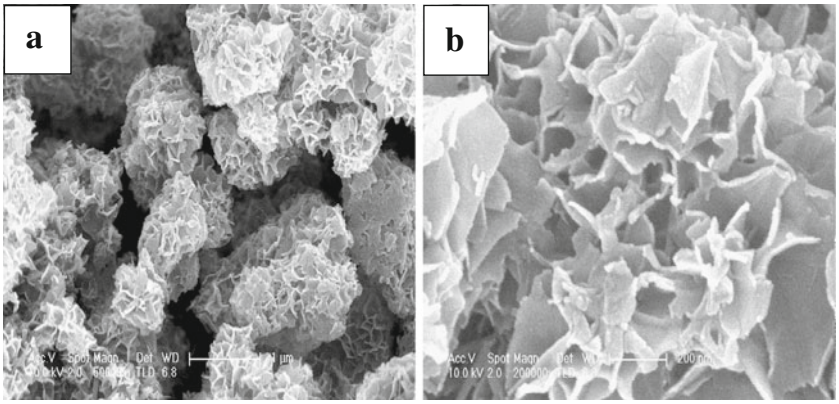

Fig. 2 SEM micrographs of MnO_2 sample S180-24 in **a** low and **b** high magnifications

indexed to the α-MnO_2 phase (JCPDS No. 44-0141). The XRD patterns show that the MnO_2 samples are poorly crystalline. The broad peaks indicate the nano-size of the MnO_2 samples or the presence of stacking defects in the samples. The sample S140-24 possesses higher crystallinity as compared to the other samples. It is interesting to notice that the transformation of poorly crystalline to crystalline nature takes place by increasing the reaction time to 24 h at 140 °C in the presence of P123. But, by subjecting $KMnO_4$ solution in the absence of P123 at 180 °C for 24 h (S180-24), only poorly crystalline α-MnO_2 is produced.

SEM and TEM studies

The morphology of MnO_2 samples was studied by SEM and TEM. The micrographs are shown in Figs. 2, 3, and 4. The SAED patterns are given as insets in the TEM images (Fig. 4). In SEM, the sample S180-24 (Fig. 2a, b) possesses a nano-layer-like morphology. Some nano-layers (Fig. 2b) aggregate together and appear as flowers (Fig. 2a) when seen under a lower magnification. The sample S140-2 consists of particles without any clear inter-particle boundary (Fig. 3a). In S140-6 sample, a combination of particles as

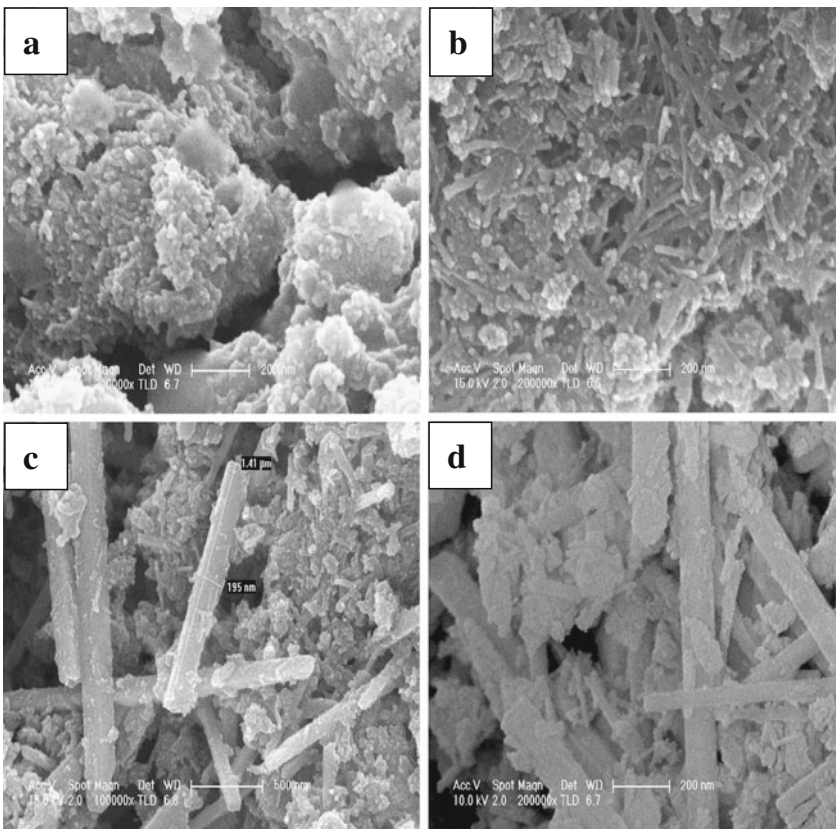

Fig. 3 SEM micrographs of MnO_2 samples: **a** S140-2, **b** S140-6, **c** S140-12, and **d** S140-24

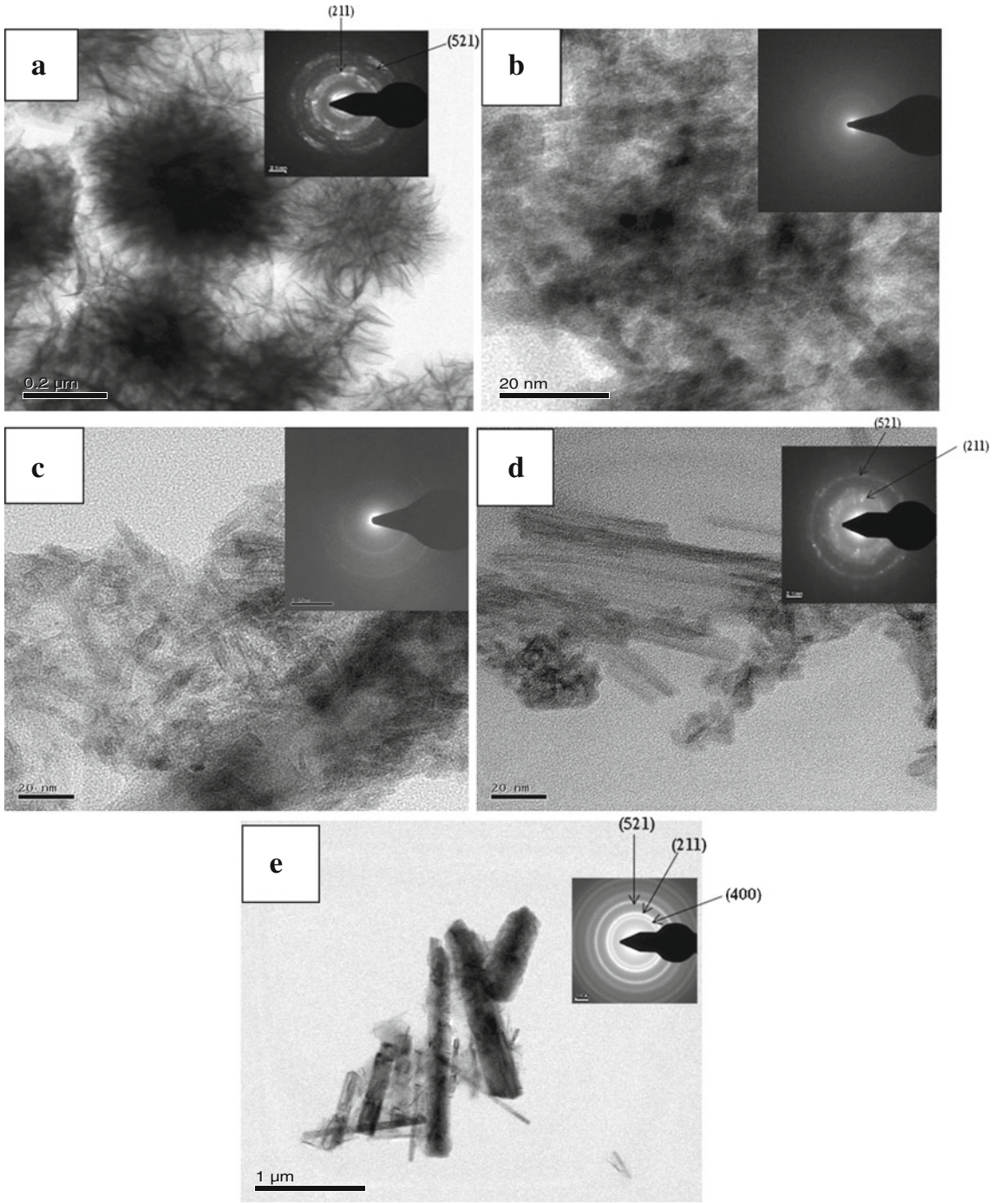

Fig. 4 TEM images of MnO_2 samples: **a** S180-24, **b** S140-2, **c** S140-6, **d** S140-12, and **e** S140-24. The SAED patterns are shown in *insets*

well as nanorods is observed (Fig. 3b). However, clear nanorods of MnO_2 are seen in SEM micrographs of S140-12 and S140-24 (Fig. 3c, d). As the reaction temperature and quantity of reactants are the same in all cases, this observation indicates that MnO_2 particles formed in 2 h duration grow and convert to nanorods by increasing the reaction time for longer than 6 h. In S140-12 and S140-24 samples, well-grown rods of about 1–2 μm in length and about 20–200 nm in diameter are observed. In TEM micrographs, similar morphologies as seen in SEM are observed for all MnO_2 samples (Fig. 4). The crystallinity of MnO_2 samples increases with an increase in reaction time of synthesis, as inferred from the SAED patterns. The SAED pattern consisting of clear rings (Fig. 4e) indicates the crystalline nature of the sample S140-24. Similar to the observations made from SEM and TEM micrographs in the present study,

changes in morphology were reported by Subramanian et al. [13] for MnO_2 samples prepared from $KMnO_4$ and $MnSO_4$ under hydrothermal conditions at 140 °C by increasing the reaction time from 1 to 18 h. Furthermore, conversion of amorphous, nanocrystalline MnO_2 to well crystalline sample was also reported [13] by increasing the reaction time, akin to the XRD patterns (Fig. 1) recorded in the present study.

Porosity measurements

N_2 adsorption–desorption isotherms with corresponding BJH pore-size distribution curves as insets for MnO_2 samples are shown in Fig. 5. The data of BET surface area, average pore diameter, and cumulative pore volume measured for all MnO_2 samples are listed in Table 1. All isotherms (Fig. 5) indicate a hysteresis between adsorption and desorption curves at high values of relative pressure suggesting that the MnO_2 samples are porous. The sample S180-24 possesses a BET surface area of 68 $m^2\ g^{-1}$. The BJH curve of sample S180-24 possesses a very narrow pore-size distribution around pore diameter of 3 nm. The pore volume is found to be 0.36 $cm^3\ g^{-1}$ (Table 1). For the samples synthesized by using P123, the specific volume of N_2 adsorbed by the samples decreases with an increase in reaction times of hydrothermal synthesis (samples S140-2 to S140-24). The volumes of N_2 adsorbed at p/p^0=0.99 are 520, 525, 450, and 212 $cm^3\ g^{-1}$ for S140-2, S140-6, S140-12, and S140-24 samples of MnO_2, respectively (Fig. 5b–e). The N_2 adsorption capacity of the sample is directly proportional to the surface area, which agrees well with the BET

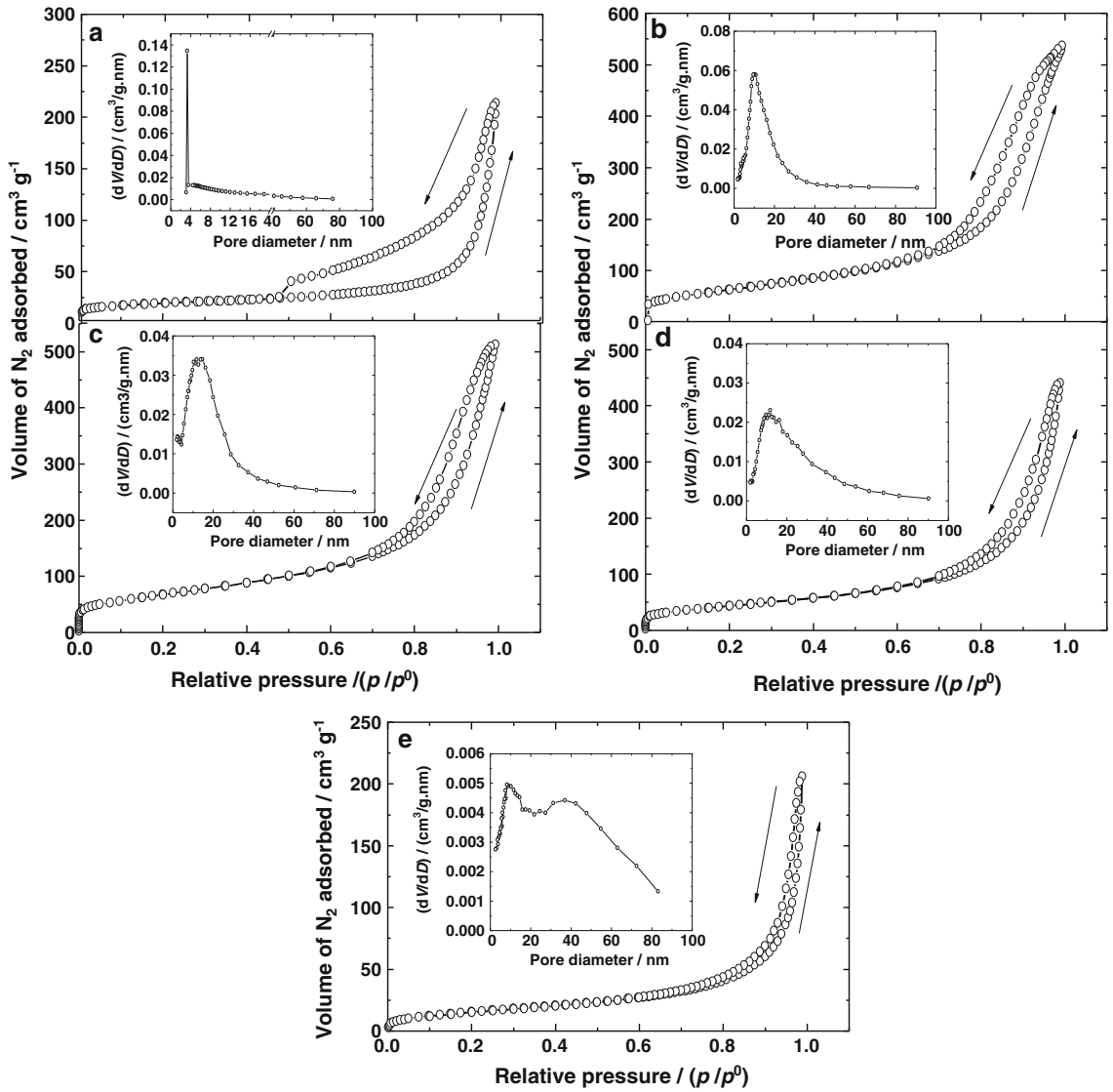

Fig. 5 N_2 adsorption–desorption isotherms with BJH pore-size distribution curves as insets of MnO_2 samples: **a** S180-24, **b** S140-2, **c** S140-6, **d** S140-12, and **e** S140-24

Table 1 Morphology, N_2 adsorption/desorption data, and discharge specific capacitance (SC) in 0.1 M Na_2SO_4 electrolyte of MnO_2 samples

Sample	Morphology	BET surface area ($m^2\ g^{-1}$)	Average pore diameter (nm)	Cumulative pore volume ($cm^3\ g^{-1}$)	SC[a] ($F\ g^{-1}$)
S180-24	Nano-layer-like	68	3.0	0.36	190
S140-2	Nanoparticle	235	12.1	0.83	185
S140-6	Nanorod	246	12.6	0.80	193
S140-12	Rod	160	15.8	0.68	135
S140-24	Rod	60	20.9	0.32	82

[a] Charge–discharge current density of 0.5 mA cm^{-2} (1.0 $A g^{-1}$)

area calculated from the adsorption isotherm (Table 1). Low values of N_2 adsorption (230 $cm^3\ g^{-1}$ for S180-24 and 212 $cm^3\ g^{-1}$ for S140-24) indicate their low surface area values. The MnO_2 samples S140-2 and S140-6 possess high BET surface areas (235–246 $m^2\ g^{-1}$) and the surface area decreases by increasing the reaction time (160 and 60 $m^2\ g^{-1}$ for S140-12 and S140-24 samples, respectively). The BET surface area values (235–246 $m^2\ g^{-1}$) are significantly greater than the values reported in the literature for MnO_2 synthesized by several routes. For instance, surface area values of 123 $m^2\ g^{-1}$ for MnO_2 synthesized in microemulsion route [3], 150 $m^2\ g^{-1}$ for hydrothermally synthesized sample [13], 108.6 $m^2\ g^{-1}$ for another hydrothermally synthesized MnO_2 [14] and 230 $m^2\ g^{-1}$ for MnO_2 prepared from reduction of $KMnO_4$ with ethylene glycol [27] were reported. The high surface area values of MnO_2 samples (S140-2 and S140-6) obtained in the present work are attributed to the presence of P123 in the reaction medium and also to the nano-size of poorly crystalline particles. For the samples prepared by subjecting the reactants for longer durations (S140-12 and S140-24), the surface area decreases (Table 1) due to change in morphology from nanoparticles to rods (Fig. 3) and also due to increased crystallinity (Fig. 1). However, the distribution of pore size becomes broader by an increase of reaction time (Fig. 5b–e insets) for the samples synthesized under hydrothermal conditions. The average pore diameter increases and cumulative pore volume decreases for these MnO_2 samples synthesized by increasing the reaction time (Table 1). These data suggest that hydrothermal reaction time exhibits a high influence on surface area, porosity, and pore volume, in addition to the morphology and crystallinity.

XPS studies

The XPS spectra of MnO_2 samples are shown in Fig. 6. The binding energies of Mn $2P_{3/2}$ and $2P_{1/2}$ at 642.2 and 653.8 eV correspond to Mn (IV) in MnO_2. All the samples possess the same binding energy for Mn 2p. This indicates that MnO_2 is stable irrespective of the hydrothermal reaction time and it is not converted to other phases such as Mn_2O_3 and Mn_3O_4 on increasing the reaction time.

Electrochemical capacitance studies

The pseudo-capacitance behavior of MnO_2 is due to a reversible redox process involving Mn^{4+} followed by surface insertion/deinsertion of cations [3, 30].

$$nMnO_2 + M^{n+} + ne^- \rightleftarrows (MnOO)_nM \quad (2)$$

where M^{n+} represents a cation. The α-form of MnO_2 consists of 2×2 tunnels (4.6 Å) [3], which can accommodate alkali or alkaline earth cations of appropriate size. The electrochemical studies of MnO_2 were reported in several electrolytes, and aqueous solution of Na_2SO_4 was found to be the suitable electrolyte for the capacitance studies because of the appropriate size of solvated Na^+ cations (4.0 Å) [3]. For this reason, 0.1 M Na_2SO_4 electrolyte was used for the electrochemical capacitance studies of MnO_2. Recently,

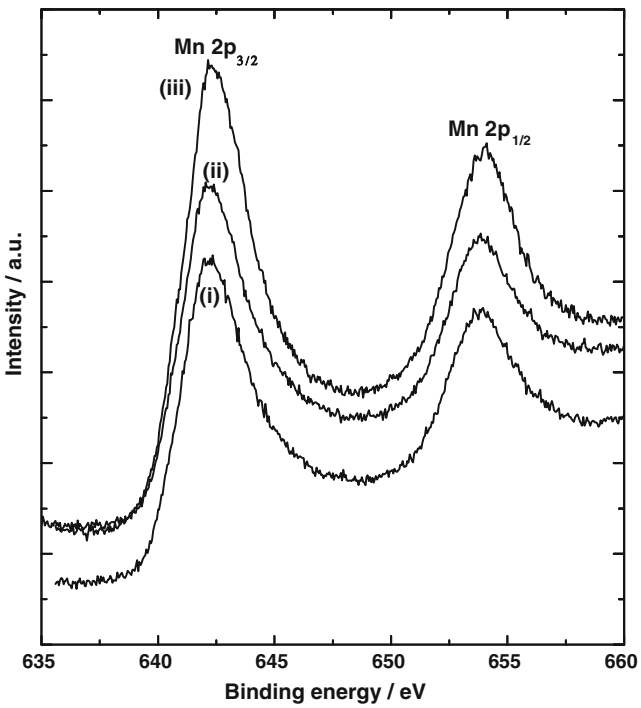

Fig. 6 XPS spectra of MnO_2 samples: *(i)* S180-24, *(ii)* S140-2, and *(iii)* S140-24

electrolytes consisting of divalent (e.g., Ca^{2+} and Mg^{2+}) and trivalent (e.g., La^{3+}) cations are also found to be useful for capacitor studies of MnO_2 [31–33].

Cyclic voltammograms (CV) of all MnO_2 samples were recorded at various sweep rates from 10 to 100 mV s^{-1} in the potential range from 0.0 to 1.0 V in 0.1 M Na_2SO_4 electrolyte, which are shown in Fig. 7. The voltammograms of all samples have the shape of a broad rectangle. The size of the rectangle increases with an increase in sweep rate for all MnO_2 samples. The rectangular shape of CV at a high sweep rate of 100 mV s^{-1} indicates a high power characteristic of the MnO_2 samples.

A few charge–discharge cycles of MnO_2 electrodes (S180-24, S140-2, S140-6, S140-12, and S140-24) at a current density (c.d.) of 0.5 mA cm^{-2} (1.0 A g^{-1}) in the potential range of 0.0–1.0 V in 0.1 M Na_2SO_4 solution are presented in Fig. 8. There is a linear variation of potential with time during charging and discharging processes, indicating the capacitance behavior of MnO_2. The discharge specific capacitance (SC) of MnO_2 was calculated using the following equation:

$$SC = I\,t/(\Delta E\,m) \tag{3}$$

where I is the charge–discharge c.d., m is the mass of MnO_2 present on the electrode, and t is the discharge time corresponding to the voltage window, ΔE (=1.0 V). The discharge SC obtained at a c.d. of 0.5 mA cm^{-2} (1.0 A g^{-1}) are 190, 185, 193, 135, and 82 F g^{-1} (Table 1) for MnO_2 samples S180-24, S140-2, S140-6, S140-12, and S140-24, respectively. The SC values are calculated on the basis of MnO_2 mass. Thus, 193 F g^{-1} obtained for S140-6 is the highest among all MnO_2 samples studied in this work. This value of SC is higher as compared to the reported values for MnO_2 synthesized by hydrothermal method [12–15]. The

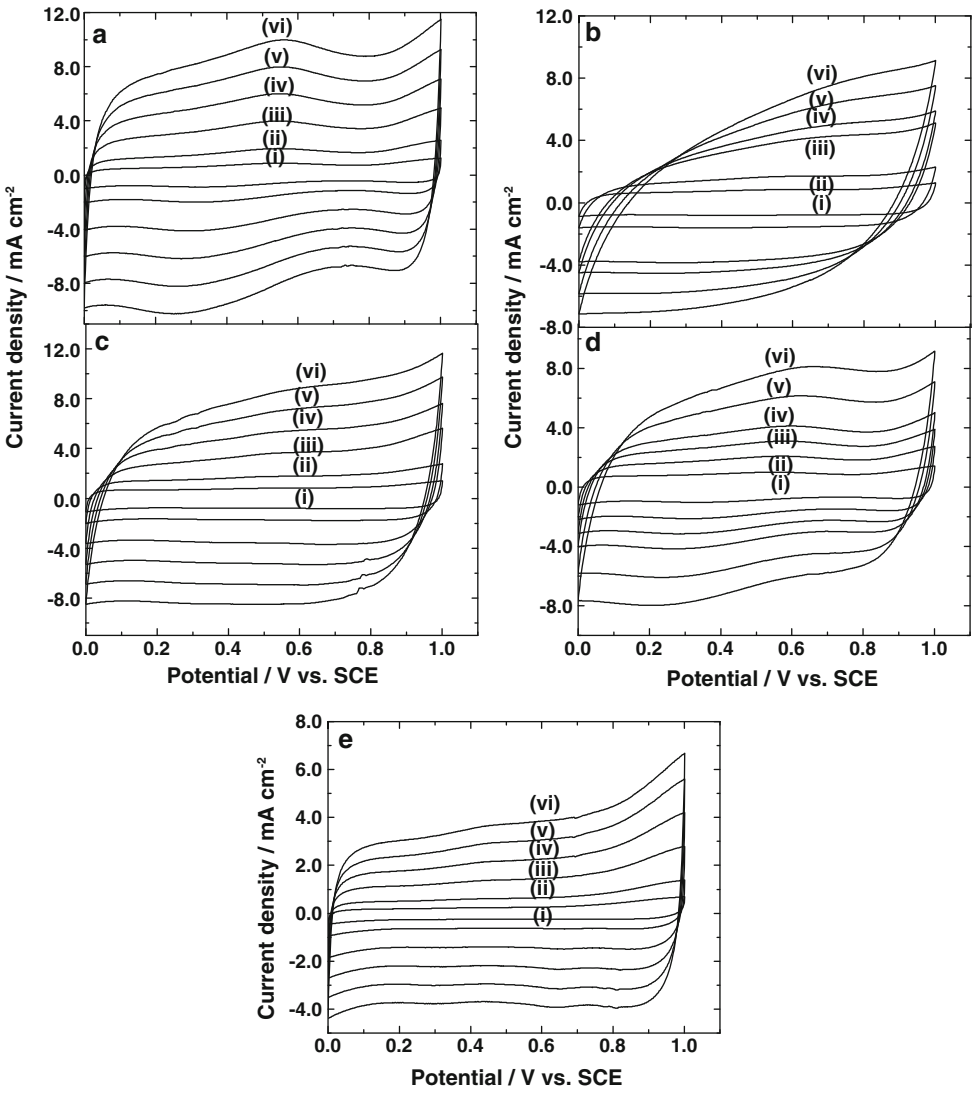

Fig. 7 Cyclic voltammograms at sweep rates of *(i)* 10, *(ii)* 20, *(iii)* 40, *(iv)* 60, *(v)* 80, and *(vi)* 100 mV s^{-1} for MnO_2 samples: **a** S180-24, **b** S140-2, **c** S140-6, **d** S140-12, and **e** S140-24 in 0.1 M Na_2SO_4 electrolyte. Area of the electrode: 1.0 cm^2, mass of MnO_2: 0.5 mg cm^{-2}

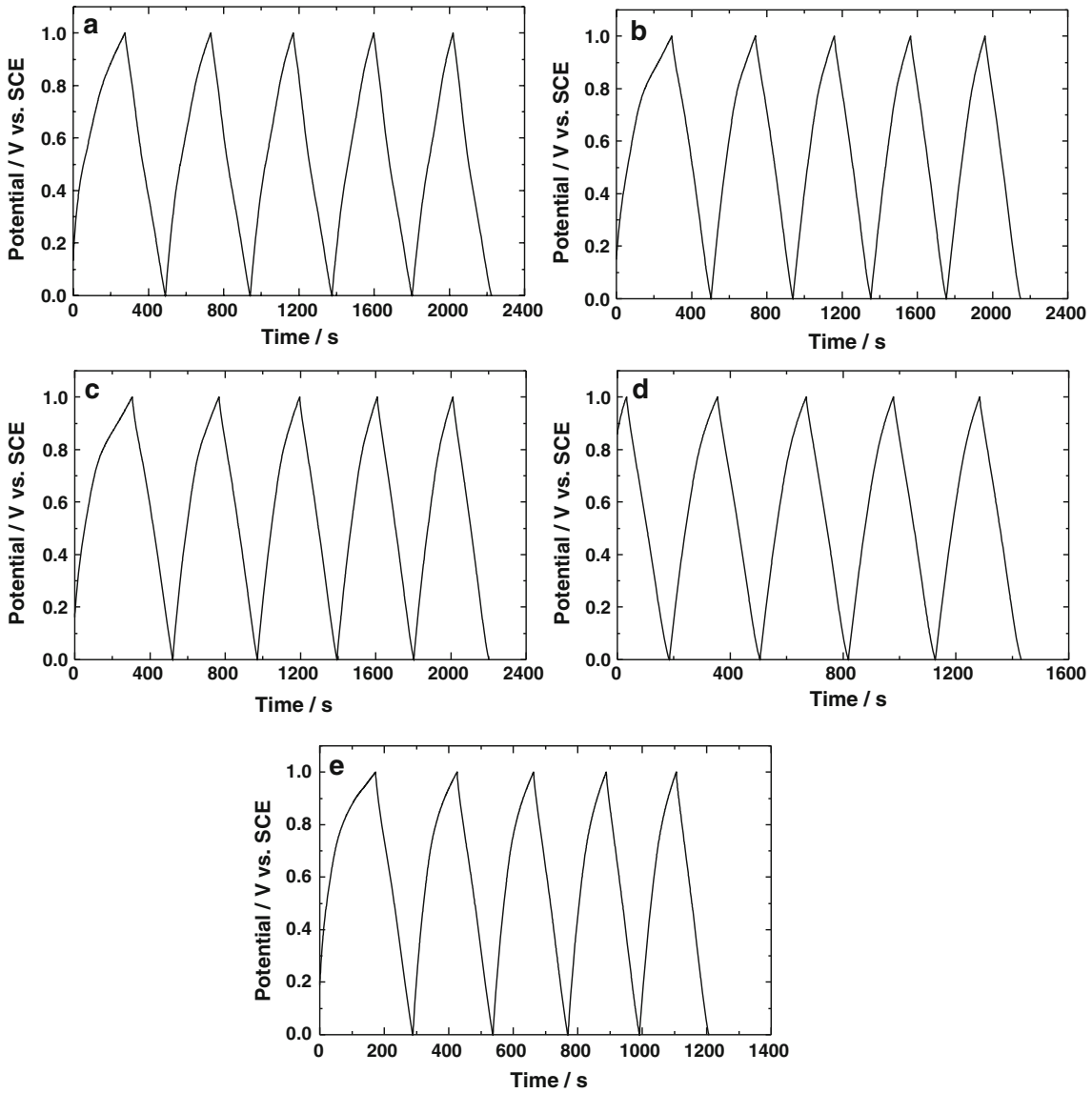

Fig. 8 A few charge–discharge cycles at a c.d. of 0.5 mA cm^{-2} (1.0 $A g^{-1}$) for MnO_2 samples: **a** S180-24, **b** S140-2, **c** S140-6, **d** S140-12, and **e** S140-24 in 0.1 M Na_2SO_4 electrolyte. Area of the electrode: 1.0 cm^2, mass of MnO_2: 0.5 mg cm^{-2}

SC value of 193 $F g^{-1}$ of MnO_2 sample (S140-6) is also higher than the SC of MnO_2 samples synthesized by co-precipitation [8] and sol–gel method [9, 10]. SC values of 134 $F g^{-1}$ by co-precipitation method [8] and 130 $F g^{-1}$ by sol–gel method [9, 10] were reported. The values of SC of MnO_2 prepared under hydrothermal conditions for durations up to 6 h (i.e., samples S140-2 and S140-6) are nearly the same (185–193 $F g^{-1}$). This is because the surface area (235–246 $m^2 g^{-1}$), average pore diameter (12.1–12.6 nm), cumulative pore volume (0.80–0.83 $cm^3 g^{-1}$), and poorly crystalline nature (Fig. 1) are nearly similar for these two MnO_2 samples. However, there is a decrease in SC by increasing the hydrothermal reaction time (Table 1) with 135 $F g^{-1}$ for S140-12 and 82 $F g^{-1}$ for S140-24 samples. The decrease in SC is attributed to a decrease in surface area and cumulative pore volume (Table 1), as well as an increase in crystallinity.

It is interesting to notice that MnO_2 prepared by hydrothermal route from $KMnO_4$ without using P123 at 180 °C for 24 h (sample S180-24) provides a SC value of 190 $F g^{-1}$ at a c.d. of 0.5 mA cm^{-2} (1.0 $A g^{-1}$), although its surface area and cumulative pore volume are low. The sample S180-24 also possesses a lower crystallinity as compared to samples S140-12 and S140-24. The high SC value of this sample is attributed to its poorly crystalline nature with nano-layer-like morphology and unique narrow pore-size distribution (3 nm). Thus, it is inferred from these studies that poor crystallinity and morphology with

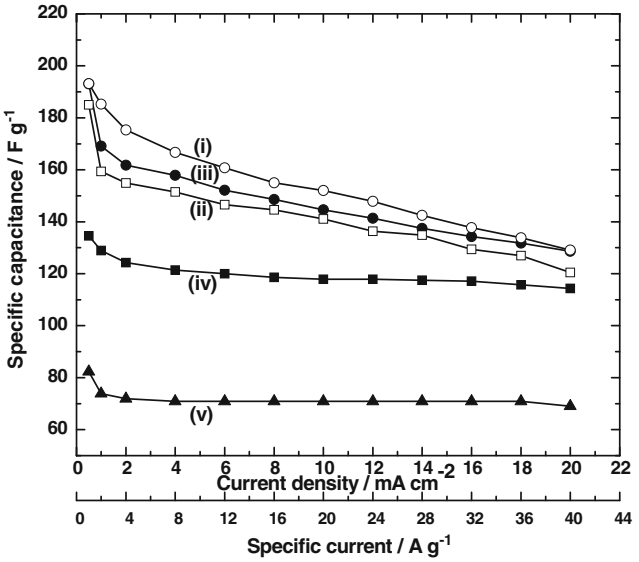

Fig. 9 Variation of SC with charge–discharge current densities for MnO_2 samples: **a** S180-24, **b** S140-2, **c** S140-6, **d** S140-12, and **e** S140-24 in 0.1 M Na_2SO_4 electrolyte. Area of the electrode: 1.0 cm^2, mass of MnO_2: 0.5 mg cm^{-2}

unique porosity plays an important role in capacitor properties of MnO_2.

In order to examine the rate capability of MnO_2, the charge–discharge cycling was carried out at different c.d.s in the range from 0.5 to 20 mA cm^{-2} (1.0 A g^{-1} to 40 A g^{-1}) in the potential window of 0.0–1.0 V in 0.1 M Na_2SO_4 electrolyte and the variation of discharge SC with an increase in c.d.s is shown in Fig. 9. With an increase in charge–discharge c.d., there is a decrease in SC for all samples of MnO_2 because of decreased utilization of the active material by the electrolyte at high c.d. values. At a high charge–discharge c.d. of 20 mA cm^{-2} (40 A g^{-1}), the discharge SC values are 119, 121, 129, 114, and 70 F g^{-1} for S180-24, S140-2, S140-6, S140-12, and S140-24, respectively. These results indicate that MnO_2 samples synthesized in the present work possess high rate capability, which is essential for a capacitor electrode material.

In order to examine the stability of the electrode material, the MnO_2 electrodes were subjected to charge–discharge cycling at a c.d. of 0.5 mA cm^{-2} (1.0 A g^{-1}) in 0.1 M Na_2SO_4 electrolyte for 1,000 cycles (Fig. 10). All MnO_2 samples are found to possess a high electrochemical stability during prolonged charge–discharge cycling. For instance, a SC of 190 F g^{-1} is obtained for the sample S180-24, which decreases to a value of 180 F g^{-1}, thus retaining 94.7% after 1,000 cycles. The sample S140-2 exhibits an initial SC of 185 F g^{-1}, which decreases to a value of 158 F g^{-1}, thus retaining 85.4% SC after 1,000 cycles. For S140-6 sample, an initial SC of 193 F g^{-1} is observed, which decreases to 182 F g^{-1}, thus retaining 94.3% capacitance after 1,000 cycles. Initial SC values of 132 and 80 F g^{-1} are obtained for samples S140-12 and S140-24, which decreases to 115 and 72 F g^{-1}, respectively, thus retaining 87.1% and 90.0% of their initial SC after 1,000 cycles. Thus, all MnO_2 samples possess high electrochemical stability in 0.1 M Na_2SO_4 electrolyte, which is essentially required for the electrochemical supercapacitors.

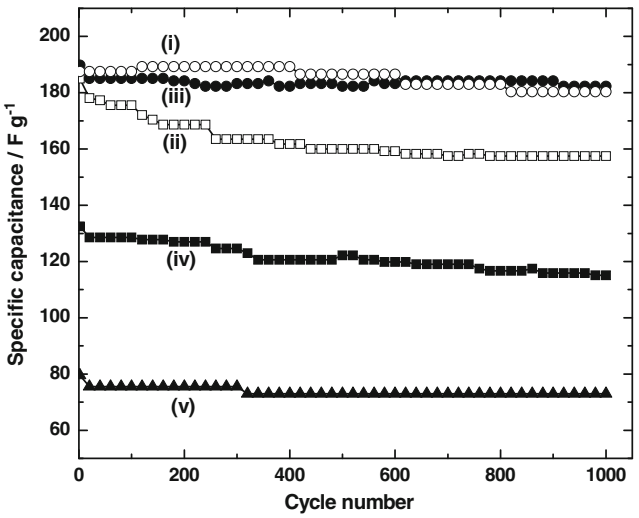

Fig. 10 Cycle-life test at a c.d. of 0.5 mA cm^{-2} (1.0 A g^{-1}) for MnO_2 samples: **a** S180-24, **b** S140-2, **c** S140-6, **d** S140-12, and **e** S140-24 in 0.1 M Na_2SO_4 electrolyte. Area of the electrode: 1.0 cm^2, mass of MnO_2: 0.5 mg cm^{-2}

Conclusions

Mesoporous MnO_2 samples are synthesized in hydrothermal method at 180 °C without using P123 and at 140 °C with P123. Changes in morphology and also in BET surface area of MnO_2 are observed with varying reaction time in hydrothermal method. Among the MnO_2 samples synthesized hydrothermally by using P123, S140-6 possesses the highest SC value of 193 F g^{-1} whereas the MnO_2 sample synthesized without using P123 (S180-24) possesses a SC of 190 F g^{-1} at a c.d. of 0.5 mA cm^{-2} (1.0 A g^{-1}). All MnO_2 samples exhibit high electrochemical stability in 0.1 M Na_2SO_4 electrolyte and hence are promising electrode materials for electrochemical supercapacitors.

References

1. Conway BE (1999) Electrochemical supercapacitors: scientific fundamentals and technological applications. Kluwer/Plenum, New York

2. Park BO, Lokhande CD, Park HS, Jung KD, Joo OS (2004) J Power Sources 134:148–152
3. Devaraj S, Munichandraiah N (2008) J Phys Chem C 112:4406–4417
4. Zhang GQ, Zhang ST (2009) J Appl Electrochem 39:1033–1038
5. Xue T, Xu CL, Zhao DD, Li XH, Li HL (2007) J Power Sources 164:953–958
6. Lee HY, Goodenough JB (1999) J Solid State Chem 144:220–223
7. Staiti P, Lufrano F (2009) J Power Sources 187:284–289
8. Lee HY, Kim SW, Lee HY (2001) Electrochem Solid-State Lett 4: A19–A22
9. Reddy RN, Reddy RG (2003) J Power Sources 124:330–337
10. Reddy RN, Reddy RG (2004) J Power Sources 132:315–320
11. Devaraj S, Munichandraiah N (2007) J Electrochem Soc 154:A80–A88
12. Subramanian V, Zhu H, Wei B (2006) J Power Sources 159:361–364
13. Subramanian V, Zhu H, Vajtai R, Ajayan PM, Wei B (2005) J Phys Chem B 109:20207–20214
14. Xu M, Kong L, Zhou W, Li H (2007) J Phys Chem C 111:19141–19147
15. Tang N, Tian X, Yang C, Pi Z (2009) Mater Res Bull 44:2062–2067
16. Xiao W, Xia H, Fu JYH, Lu L (2009) J Power Sources 193:935–938
17. Chen R, Javaliz P, Whittingham MS (1996) Chem Mater 8:1275–1280
18. Hu CC, Tsou TW (2002) Electrochem Commun 4:105–109
19. Pang SC, Anderson MA, Chapman TW (2000) J Electrochem Soc 147:444–450
20. Devaraj S, Munichandraiah N (2005) Electrochem Solid-State Lett 8:A373–A377
21. Hu CC, Wang CC (2003) J Electrochem Soc 150:A1079–A1084
22. Du G, Wang J, Guo Z, Chen Z, Liu H (2011) Mater Lett 65:1319–1322
23. Muth O, Schellbach C, Froba M (2001) Chem Commun 2032–2033
24. Hayashi H, Hakuta Y (2010) Materials 3:3794–3817
25. Jiang R, Huang T, Liu J, Zhuang J, Yu A (2009) Electrochim Acta 54:3047–3052
26. Jeong YU, Manthiram A (2002) J Electrochem Soc 149:A1419–A1422
27. Ragupathy P, Park DH, Campet G, Vasan HN, Hwang SJ, Choy JH, Munichandraiah N (2009) J Phys Chem C 113:6303–6309
28. Subramanian V, Zhu H, Wei B (2008) Chem Phys Lett 453:242–249
29. Nayak PK, Munichandraiah N (2011) Microporous Mesoporous Mater 143:206–214
30. Toupin M, Brousse T, Belanger D (2004) Chem Mater 16:3184–3190
31. Xu C, Du H, Li B, Kang F, Zeng Y (2009) J Electrochem Soc 156: A73–A78
32. Xu C, Du H, Li B, Kang F, Zeng Y (2009) J Electrochem Soc 156: A435–A441
33. Nayak PK, Munichandraiah N (2011) J Electrochem Soc 158: A585–A591
34. Kim JH, Zhu K, Yan Y, Perkins CL, Frank AJ (2010) Nano Lett 10:4099–4104
35. Hasan M, Jamal M, Razeeb KM (2012) Electrochim Acta 60:193–200
36. Xia XH, Tu JP, Wang XL, Gu CD, Zhao XB (2011) Chem Commun 47:5786–5788
37. Mu J, Chen B, Guo Z, Zhang M, Zhang Z, Zhang P, Shao C, Liu Y (2011) Nanoscale 3:5034–5040
38. Wee G, Soh HZ, Cheah YL, Mhaisalkar SG, Srinivasan M (2010) J Mater Chem 20:6720–6725